Understanding the stability mechanism of silica nanoparticles
The effect of cations and EOR chemicals

Liu, Zilong; Bode, Vincent; Hadayati, Pegah; Onay, Hayati; Sudhölter, Ernst J.R.

DOI
10.1016/j.fuel.2020.118650

Publication date
2020

Document Version
Final published version

Published in
Fuel

Fuel 280 (2020) 118650

Contents lists available at ScienceDirect

Fuel

journal homepage: www.elsevier.com/locate/fuel

Full Length Article

Understanding the stability mechanism of silica nanoparticles: The effect of cations and EOR chemicals

Zilong Liu*, Vincent Bode, Pegah Hadayati, Hayati Onay, Ernst J.R. Sudhölter*

Organic Materials & Interfaces, Department of Chemical Engineering, Faculty of Applied Sciences, Delft University of Technology, Van der Maasweg 9, 2629 HZ Delft, the Netherlands

ARTICLE INFO

Keywords:
Silica nanoparticle
Salt solution
Surfactant
Polyelectrolyte
Enhanced oil recovery

ABSTRACT

We have investigated the conditions of colloidal stability of silica nanoparticles smaller than 100 nm for their applications in enhanced oil recovery (EOR), especially pertaining to chemical flooding processes. Using zeta sizer and dynamic light scattering techniques, the stability of silica nanoparticle (SNP) dispersions has been investigated by variation of the pH, composition of salt solutions, addition of surfactants and polyelectrolytes. Such conditions can be encountered in oil reservoirs. It was found that changing pH from 5 to 10 had a negligible effect on the size of SNPs, whereas its zeta potential increased with increasing pH. Aggregation of SNPs is a partially reversible process for low degrees of aggregation in 500 mM NaCl, whereas observed strong aggregation in 1000 mM NaCl was irreversible. A critical aggregation concentration (CAC) was defined for the different salts investigated, above which the SNP dispersion became unstable at a fixed pH of 9.5. The CAC for NaCl was approximately 200 times higher than for $CaCl_2$ and $MgCl_2$. Our observations could not be explained completely by the Derjaguin-Landau-Verwey-Overbeek (DLVO) theory. Therefore, we have included non-DLVO interactions such as cation bridging, hydration forces, and steric effects. The additional presence of anionic alcohol alkoxy sulfate (AAS) surfactant slightly destabilized the SNP solution, but by the addition of polyacrylate (PA) was effectively stabilized. With increasing PA concentration, the CAC for both $CaCl_2$ and $MgCl_2$ increased. Upon addition of 100 ppm PA, the CAC increased by a factor of five compared to the situation in the absence of PA. Reducing the solution pH below 8.5, SNP can be stabilized in higher salinity in the presence of PA. The obtained results contribute to a better fundamental understanding of the SNP stability mechanism and a guide to optimize the SNP injection process with EOR chemicals.

1. Introduction

Owing to the increased demand for energy, it is extremely important to maximize oil recovery yields before abandoning existing wells to newly discovered ones [1–3]. To efficiently recover bypassed oil and residual oil trapped in the reservoir, numerous enhanced oil recovery (EOR) technologies have risen in the last few decades [4]. Among them, a better recovery can be achieved by chemical EOR (cEOR). It involves injecting a variety of chemicals such as alkali, surfactant, and polymer. Surfactants are frequently used to lower the oil-water interfacial tension (IFT), alter the rock wettability, generate emulsion, and stabilize foam [5–9]. On the other hand, polymers attempt to increase the viscosity of injected solutions, and therefore improve the mobility ratio and volumetric sweep efficiency of the reservoir [4,10], whereas alkalis increase pH, reduce adsorption of anionic surfactants, activate the reaction with an acidic constituent in crude oil, and facilitate the generation of in situ surfactants [11]. Although various cEOR methods were found to be effective and successfully applied in the oil fields, their applications are limited in high salinity and high hardness conditions, and challenged with surfactant losses by adsorption to rock surfaces [12–14].

Recently, there has been a growing interest in the utilization of nanoparticles (NPs) with other chemicals, which shows potential to address challenges caused by traditional cEOR methods [10,15–19]. It has been shown that a NP dispersed solution was able to alter the wettability of the rocks towards water-wet and reduce the oil-water IFT [14,20,21]. Adding NPs resulted in a lower anionic surfactant adsorption on rock surfaces [18]. NPs can also be used to stabilize emulsion by overcoming the challenges encountered by other stabilizers such as surfactants [22]. Moreover, NPs treatment of low salinity water flooding was able to prevent fines migration in the reservoir [23]. NP dispersions displaced crude oil with the structural disjoining pressure mechanism [24]. The stability of NP-surfactant foam was enhanced by

* Corresponding authors.
E-mail addresses: zlliu89@gmail.com (Z. Liu), E.J.R.Sudholter@tudelft.nl (E.J.R. Sudhölter).

https://doi.org/10.1016/j.fuel.2020.118650
Received 20 May 2020; Received in revised form 23 June 2020; Accepted 5 July 2020
Available online 17 July 2020

the adsorption and accumulation of NPs at the foam lamellae [25]. Additionally, most NPs applied in EOR are environmentally friendly, especially for silica NPs (SNPs) that are compatible with sandstone reservoirs. Because of the extremely small size of NPs that ranges from 1 to 100 nm, they can easily propagate through porous formations with low or no retention [1,2]. Depending on size and shape, NPs exhibit exceptional thermal, rheology, magnetic and stress-strain properties [26,27]. Furthermore, NPs can be produced with great control, their physical-chemical properties are very well known, and their surface can be readily functionalized by the grafting of terminal groups [28]. Besides, in the carbon geosequestration field, amine-based nanoparticle suspensions and nanoparticle organic hybrid materials have been developed for CO_2 capture that is also important to the CO_2 flooding on oil production [29–31].

In order to reap the benefits of NPs in EOR, one of the most important challenges is the stability of NPs in an aqueous solution. Thermodynamically, NPs tend to aggregate to reduce the large surface energy. This aggregation is governed by interparticle collisions, which occur as a result of Brownian motion that the NPs are continuously subjected to [32]. Particle size increase could lead to loss of NPs original characteristics and block pore throats [10]. In the majority of recent EOR studies, NPs were widely applied in deionized water, dilute brine at very low ionic strength, or low divalent cation solutions [14,33–38]. However, water flooding and EOR projects typically use seawater or formation water, containing multiple types and charges of ions. Under such saline environments, concentrated electrolytes (*e.g.* NaCl, $CaCl_2$, and $MgCl_2$) can dramatically accelerate particle flocculation and coagulation because of the increased rate of collision and coalescence of NPs [39]. Besides, the influence of injected chemicals (*e.g.* surfactants and polymers) on the dispersion and stability of NPs are not well understood [36,40–42]. As a result, it is very crucial to understand the stability of NPs in the aqueous phase and generate homogeneous NPs dispersions.

During the Brownian motion of NPs in different fluids, their stabilities are determined by integration of the attraction and repulsion forces between the NP surfaces. The six most important interactions that exist through the medium can be separated into three attractive interactions (van der Waals (vdW) interaction, cation bridging, and hydrophobic forces) and three repulsive forces (electric double layer (EDL) forces, steric hindrances, and hydration forces), with the total sum of six governing the overall stability of the solution. To maintain a stable dispersion, these repulsive forces need to be sufficiently larger than the attractive forces in order to overcome the inherent instability [43,44]. However, before this stability can be assessed, the term stability, and by extension stable and unstable, should be defined clearly. Ideally, this would be done by looking at the pore throat blocking which can result from the NP aggregation. Instead, the pore throat size of conventional sandstone and carbonate reservoirs is used as a measure, typically 2 μm or larger [45], with the NPs needing to be much smaller. With this, and the definition of nanoscale (particles with sizes ranging from 1 to 100 nm) [46], the common limit for NP stability is taken therefore to be 100 nm.

In this study, we have systematically investigated the effect of cations and EOR chemicals on the stability of SNP dispersions. By measuring the zeta potential and particle size of various SNP dispersions in the presence of salt, the stability of SNP was quantitatively evaluated. This has been done by finding the critical aggregation concentration (CAC), defined as the salt concentrations at which the SNP solution becomes unstable. If the diameter of the aggregated SNP is above 100 nm, SNP solution is considered to be unstable and should not be used for EOR injections because it could block pore throats. One of our aims was to gain insights into the processes that control the stability behaviour under the conditions of the monovalent cation (NaCl), divalent cations ($CaCl_2$ and $MgCl_2$), commonly used anionic surfactant alcohol alkoxy sulfate (AAS), and the anionic polyelectrolyte polyacrylate (PA). We also examined our data in light of the Derjaguin-Landau-Verwey-Overbeek (DLVO) theory, but it could not account for the salinity dependent aggregation. The importance of non-DLVO interactions such as cation bridging, hydration forces, and steric effects was highlighted for the understanding of SNP stability. This is very important to reveal the underlying stability mechanisms of SNP dispersions, in order to contribute to improved SNP injections used in EOR.

2. Experimental methods

2.1. Chemicals and solutions

Two types of Ludox colloidal suspensions of SNPs, 40 wt% HS-40 (1.3 g/mL, 0.52 g SiO_2/mL) and 45 wt% CL-X (1.36 g/mL, 0.61 g SiO_2/mL) in water, were purchased from Sigma Aldrich. These HS-40 and CL-X SNPs had average diameters of 12 and 20 nm (as measured by atomic force spectroscopy), respectively. The surface area determined with Brunauer-Emmett-Teller (BET) was about 220 m^2/g for HS-40 and 130 m^2/g for CL-X. Two stock solutions were made by diluting 6.22 mL HS-40 and 5.24 mL CL-X each with 100 mL of distilled water (MILLI-Q with a resistivity of > 18.2 MΩ·cm) giving a 3.0 wt-% stock solution for each SNP.

Sodium chloride (BioUltra, for molecular biology, ≥99.5% (AT)), magnesium chloride (hexahydrate, 'Baker Analyzed'), and calcium chloride (dihydrate, ACS reagent, ≥99%) were purchased from Sigma Aldrich. From these, three 500 mL stock solutions were made by dissolving 58.46 g NaCl (2 M), 10.17 g $MgCl_2$ (100 mM), and 7.36 g $CaCl_2$ (100 mM) in MILLI-Q. The anionic AAS surfactant (Enordet J771) having a molecular weight (MW) of 700 g/Mol was provided by Shell Global Solutions. This surfactant contained mainly C_{12}/C_{13} alkyl tails connected *via* seven propoxy units to a sulfate head group. Such an AAS surfactant is commonly used in cEOR with excellent divalent cation tolerance and is relatively inexpensive in comparison with other types of EOR surfactants [47]. A 15 wt% stock solution of AAS (0.99 g/mL, 0.15 g AAS/mL) was used. Lastly, a 45 wt% poly(acrylic acid, sodium salt) (PA) (1.32 g/mL, 0.59 g PA/mL), was purchased from Sigma Aldrich. The PA is an anionic polyelectrolyte and had a mean MW of 1200 g/Mol, giving a mean monomer count of 16. A 600 ppm stock solution was made by diluting 6.71 mL of these commercial solutions with 100 mL MILLI-Q water. All of the solutions described below were, unless stated otherwise, made by mixing and/or diluting the above described stock solutions.

2.2. Measurements

2.2.1. Visual inspections

In the first step, all SNP solutions were evaluated visually against a black background. The duration of this step was 48 h and the purpose was to examine the turbidity and possible precipitations in the solutions. If no precipitation or severe cloudiness was observed, we will go to the second step to measure the size and zeta potential distribution of the SNP solutions. Otherwise, the solution was deemed visually unstable, and no measurements were performed.

2.2.2. Size measurements

Dynamic Light Scattering (DLS) is a commonly used method to measure the hydrodynamic size of particles in solution. The DLS measurement was performed at a fixed backscatter angle of 173° with a Malvern Zetasizer Nanoseries ZS, in disposable micro cuvettes. For each measurement, one milliliter of the sample was used, and each measurement was performed three times (with 12 runs per measurement) on the same sample. This gave size distribution of the solutions, the intensity-weighted average of which was reported. All SNP-salt combinations (*e.g.* HS-40 with NaCl, CL-X with NaCl, HS-40 with $MgCl_2$) were measured in separate cuvettes, in order to minimize the risk of cross-contamination. These cuvettes were rinsed thrice with MILLI-Q

between measurements, and each series of measurements was performed in the order of increasing salt concentration.

2.2.3. Zeta potential measurements

The laser Doppler electrophoresis (LDE) was performed using the same Zetasizer as the DLS, but with DTS 1070 zeta potential cells from Malvern. The cells were rinsed with MILLI-Q between measurements. Then, two millilitres of the sample were inserted into the cell, displacing the water and assuring the cell was fully filled. Then, the cell was lightly tapped to dislodge any air bubbles present in the solution. While a separate cell was used for each salt, there were no separate cells for the SNPs (*e.g.* the NaCl cell measured both HS-40 with NaCl, and CL-X with NaCl). Measurements series were performed in increasing order of salt concentration, with four measurements per sample, the intensity-weighted average of which was reported.

2.3. pH effects

Two identical 40 mL solutions of 0.3 wt% HS-40 in MILLI-Q were made in 50 mL plastic centrifuge tubes. These solutions were sonicated in a VWR Ultrasonic Cleaner USC-TH for 15 min at room temperature. Then, the pH of both solutions was measured with a Metrohm 827 pH lab, and one solution was brought to a pH of 10 by adding drops of diluted NaOH. The size and zeta potential distribution of this solution was then measured immediately, and while these measurements were in progress, the pH of the second solution was brought to 9 using diluted HCl. This process was then repeated in HS-40 solutions for pH 8, 7, 6, 5 and for CL-X.

2.4. Salt effects

40 mL 0.3 wt% SNP solutions with varying salt concentrations were made batch-wise in batches of four solutions by mixing pre-determined amounts of salt stocks, MILLI-Q, and SNP stocks. Then, one sample at a time, the pH of each solution was measured and adjusted to 9.5 because this pH resembles practical alkaline conditions in cEOR. Once all four solutions were made, the samples were sonicated simultaneously. Note that all samples described below were sonicated before the salt was added. Here, we were also interested to check the reversibility of the aggregation of SNPs. Two 40 mL solutions of 0.3 wt% HS-40 were made, one in 1000 mM NaCl, and the other in 500 mM NaCl. The solutions were left to set for 72 h, after which the solutions were overturned, shaken, and both diluted with MILLI-Q and HS-40 stock solution into a pair of two 0.3 wt% HS-40 in 100 mM NaCl solutions. The pH of these solutions was again adjusted to 9.5, and of each pair, one solution was sonicated while the other was not.

2.5. AAS/PA effects

40 mL solutions containing 0.3 wt% SNP, varying salt concentrations, and additives (0.15 wt% AAS or 30, 60, or 100 ppm PA) were made by first diluting the SNP stock with MILLI-Q. The concentration AAS chosen was above its critical micelle concentration, which was typically used cEOR. A higher concentration PA stock (1600 ppm) was made by diluting 12.54 mL of commercial PA solution with 70 mL MILLI-Q. With this stock, 40 mL solutions containing 0.3 wt% HS-40, 50 mM $MgCl_2$, and 250, 500, 750, and 1000 ppm PA were made. These solutions were then sonicated, and the additive stock was added. To fully disperse this additive, the solutions were shaken for 15 min in a Scientific Instruments Vortex Genie 2 at the power setting 4 (out of 10). After shaking, the salt stock was added, and the pH was brought to 9.5. In addition, the pH effect of 0.3 wt% HS-40 solutions in the presence of 50 mM $CaCl_2$ with 300 ppm PA was examined.

2.6. Stability mechanisms

2.6.1. DLVO theory

The DLVO theory is widely applied to the interaction between two charged surfaces in a liquid medium, such as salt solutions. Based on DLVO modelling, the basic assumption is that the particles are spherical. DLVO theory implies that the stability of spherical NPs in dispersions is evaluated by the sum of attractive vdW (E_{vdW}) and repulsive EDL (E_{EDL}) interactions:

$$E_{DLVO} = E_{vdW} + E_{EDL} \tag{1}$$

The vdW interaction is a general label given to a set of interparticle attractive forces consisting of dipole-dipole, dipole-induced dipole, and instantaneously induced dipole-induced dipole interactions (the last one is also called London dispersion force). This interaction energy between two identical spherical particles of radius r whose surfaces are separated by a distance D can be calculated using the following expression [48]:

$$E_{vdW} = -\frac{A}{6}\left[\frac{2r^2}{(4r+D)D} + \frac{2r^2}{(2r+D)^2} + ln\frac{(4r+D)D}{(2r+D)^2}\right] \tag{2}$$

where A is the Hamaker constant. For SNPs in water, the effective Hamaker constant was reported to be 3.6×10^{-21} J [49].

Due to the oxygen-containing silanol groups on the surface, silica can be protonated or deprotonated when brought into aqueous solutions. Because of the resulting surface charge, an EDL will form around the surface of charged particles when they are introduced into an aqueous electrolyte solution. It consists of two layers, a compact Stern layer of the charged surface and associated counterions, and a diffuse layer consisting of counterions drawn towards the particle by the Coulomb interactions between them. A distinction can be made between ions that move with the SNP (in the EDL), and the ions that do not (in the bulk). The plane between these two is called the slipping plane (note that this is not necessarily the end of the diffuse layer). The potential at this slipping plane is called the zeta potential [50], and acts as an effective particle charge. It is impossible to directly measure the NPs surface charge, and as a result, the zeta potential is measured instead and taken as a measure for the surface charge. The thickness of the EDL is called the Debye length. This length (k^{-1}) is given, in nanometer, by

$$k^{-1} = \sqrt{\frac{\varepsilon_r \varepsilon_0 k_B T}{\sum \rho_{\infty i} e^2 z_i{}^2}} \tag{3}$$

where e is the elementary charge of an electron, z represents its valence, ε_0 and ε_r are the absolute and solution relative dielectric constants respectively, k_B is the Boltzmann constant, T represents the absolute temperature in Kelvin, and $\rho_{\infty i}$ is the number density of ion i in the bulk solution. The Debye length can then be used to determine the electrostatic double layer interaction between two equally sized spherical NPs [48]:

$$E_{EDL} = (64\pi k_B T r \rho_\infty \gamma^2/k^2) e^{-kD} \tag{4}$$

with γ the reduced surface potential, which is obtained from

$$\gamma = \tanh\left(\frac{zeE_0}{4k_B T}\right) \tag{5}$$

where E_0 is the surface potential. If the surface potential E_0 is below about 25 mV, the Eq. (4) simplifies to the following [48]:

$$E_{EDL} \approx 2\pi\varepsilon_r \varepsilon_0 r E_0{}^2 e^{-kD} \tag{6}$$

2.6.2. Non-DLVO theory

The DLVO theory often fails to accurately predict the stability of strongly hydrophobic or hydrophilic particles, or solutions comprising multivalent ions, especially those with high ionic strength [51].

Additionally, most explanations of DLVO theory explicitly state that it is only accurate in the absence of surfactants or polymers. All this can be attributed to influences from non-DLVO interactions that work in addition to the two explained above. In the case of hydrophilic SNP dispersions with high ionic strength, hydration repulsion energy and cation bridging can be considerable, and hydrophobic interactions are excluded. As particle collisions require interpenetration of grafted molecule layers, the steric effect is also relevant, but will not be discussed in depth. In addition, the proton protection method for the stabilization of SNP is also introduced.

2.6.2.1. Hydration force. If a hydrophilic particle is introduced into an aqueous environment, a thin layer of physically bound water will be formed around it, made out of water molecules associated with the particle. Strongly hydrophilic particles, like the SNP used in this research, can have large amounts of 'bound water', to the point where it can significantly affect the interaction between the particles, and by extension, the stability of the solution. However, it has been shown that the presence of cations disrupts this ordering of water molecules [52]. When two hydrated surfaces approach each other, the collision will be hindered by an additional repulsive force, separate from the EDL. This repulsion arises from the fact that, in order for the surfaces to truly make contact, the 'bound water' molecules need to be displaced, which requires additional work and hence increases the free energy of the system.

2.6.2.2. Cation bridging. It has been shown that multivalent cations can form 'cation bridges' between negatively charged surfaces and negatively charged molecules [53]. In the presence of both monovalent and multivalent cations, Higgins and Novak have shown that there is competition, as the addition of sodium ions reduced the extent of flocculation caused by multivalent cations [54]. If the total concentration of monovalent cation was more than twice the total concentration of divalent cation, then the flocculation was greatly deteriorated [54]. Following the same mechanism, polyelectrolytes can also form interparticle bridges, because of their multivalency. However, this was only prevalently observed in solutions containing low concentrations of very large polymers, with molecular weights in the millions [55]. It is due to the polyelectrolytes having to bind to two different nanoparticles to form a 'bridge'. But in solutions with higher concentrations, it is much more likely for each polyelectrolyte to only bind to one particle, as the surface will be covered to such an extent where there is insufficient room for another particle's polyelectrolyte to bind.

2.6.2.3. Proton protection. To minimize the binding of divalent cations to SNP, Sofla et al. [56] introduced a much weaker, less destabilizing cation, H^+, which can compete with the cations from the solution. This can be simply achieved by lowering the pH of the solution. After increasing the pH towards neutral conditions, these protons still make up a large portion of the Stern layer. Listed advantages of this method is the lower price of HCl compared to the use of surfactants or polymers, as well as avoiding hydrolysis of surfactants and polymers at higher temperatures. The disadvantages are the possibilities of unwanted secondary effects as a result of the lower pH (*e.g.* mineral dissolution), and the fact that the protons will be removed from the Stern layer at higher pH, requiring the solution to remain acidic or neutral.

3. Results and discussion

3.1. Effect of pH

The effect of pH ranging from 5 to 10 on the size and zeta potential of both SNPs is shown in Fig. 1. There was no significant effect on the size of SNPs, with average hydrodynamic sizes of 23–24 nm. However, the zeta potential of SNPs was substantially affected, which was expected, as silanol groups of SNPs can be deprotonated because SNP have two pKa's of 4.5–5.5 and 8.5–9.9 [57]. The zeta potential value of HS-40 ranged from −29 to −58 mV and CL-X showed the values from −31 to −46 mV over pH 5–10. The change of zeta potential was steep for HS-40 at higher pH and this can be attributed to its larger surface area, with more silanol groups to be deprotonated. Likewise, at a lower pH, it was more protonated, explaining the lower zeta potential compared to CL-X. Despite this protonation, both HS-40 and CL-X were still negatively charged at all investigated pH values.

However, the zeta potential decreased (became less negative), one would initially expect an accompanying increase in size, but this was not observed. The lack of correlation between the two parameters can be explained by the DLVO theory. Although the repulsive EDL force (proportional to the zeta potential) became weaker, there is no considerable aggregation expected as long as the decreased repulsive EDL interaction is larger than the attractive vdW force. It should be noted that solutions were not necessarily more stable at higher pH. After the salt was added, the initially stable solution could start aggregating as the pH was higher.

3.2. Effect of various salt solutions

3.2.1. NaCl solution

Fig. 2 shows the behaviour of SNPs at room temperature, pH = 9.5 and in the presence of NaCl. A typical phase behavior of SNP dispersions with varying NaCl concentrations after 48 h was observed and shown in Fig. 2a. The addition of NaCl up to 600 mM did not destabilize the aqueous dispersion of HS-40. The solution was clear and there was no serious cloudiness. However, with further increasing concentrations of NaCl (700 to 850 mM), the initial solutions became cloudy and finally produced SNP precipitations. As stated in Section 2.2.1, only stable and clear dispersions would be used for later measurements. The size and zeta potential of SNPs in the solutions comprising different NaCl concentrations were studied and the obtained results were compared with the DLVO theory (Fig. 2b–d). These plots nicely illustrated the general shapes of the size and zeta potential curves that took over the course of this research. The size of both SNPs started nearly constant, with only a slight slope at higher concentrations, followed by a rapid increase as the particles started obviously aggregating. At NaCl concentration of 600 mM, the size of HS-40 was 104 ± 2 nm that approached to limited SNP size of 100 nm. The 500–600 mM can be considered as the CAC for HS-40 in the presence of NaCl. Whereas, the CL-X was observed to aggregate later than the HS-40, as it had a higher CAC of 750–800 mM in Table 1. This could be the result of the smaller surface area of CL-X, as they therefore had less negative groups, and a weaker electrostatic repulsion (smaller zeta potential) as compared to HS-40. In Fig. 2c, the zeta potential exhibited an opposite behaviour to sizes, considerably decreasing at low concentrations, and then flattening out, a behaviour caused by the formation and subsequent filling of the EDL. At the point where the SNPs rapidly started aggregating (around 400 mM for HS-40 and 600 mM for CL-X), the zeta potential nearly kept constant (other than the outlier at 700 mM for CL-X). If zeta potential reached the plateau, the repulsive EDL interaction among SNPs kept constant and the aggregation seemed to easily occur.

To explain the stability of SNPs in the presence of NaCl, the obtained results of size and zeta potentials were modelled with DLVO theory (Section 2.6) and the results are exhibited in Fig. 2d. The positive energy indicates a repulsive interaction and the negative energy is an attractive interaction. DLVO calculations showed that there was a relatively large repulsive energy barrier for the aggregation of both HS-40 and CL-X. The repulsive EDL interaction was larger than attractive vdW interaction between SNPs for a wide range of distances. In 10 mM NaCl, the value of repulsive energy barrier was about 3 times more than in 100 NaCl. The size of both SNPs was similar, indicating that the vdW interaction almost equally contributed to the DLVO energy. The EDL

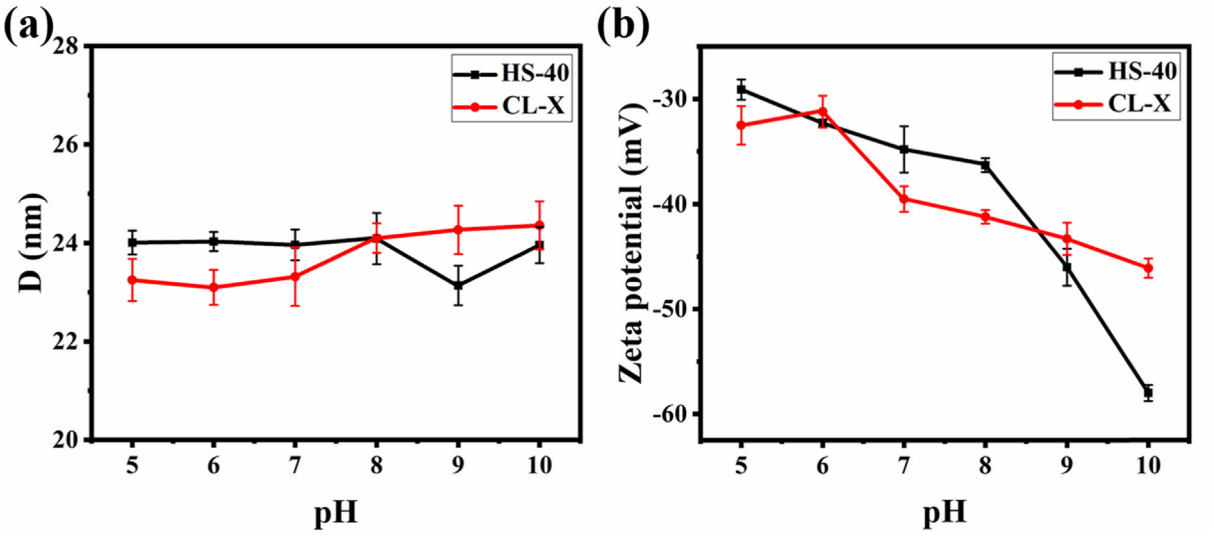

Fig. 1. (a) DLS analysis of size and (b) LDE zeta potential of HS-40 and CL-X silica nanoparticles dispersed in the aqueous solution with varying pH, at ambient temperature.

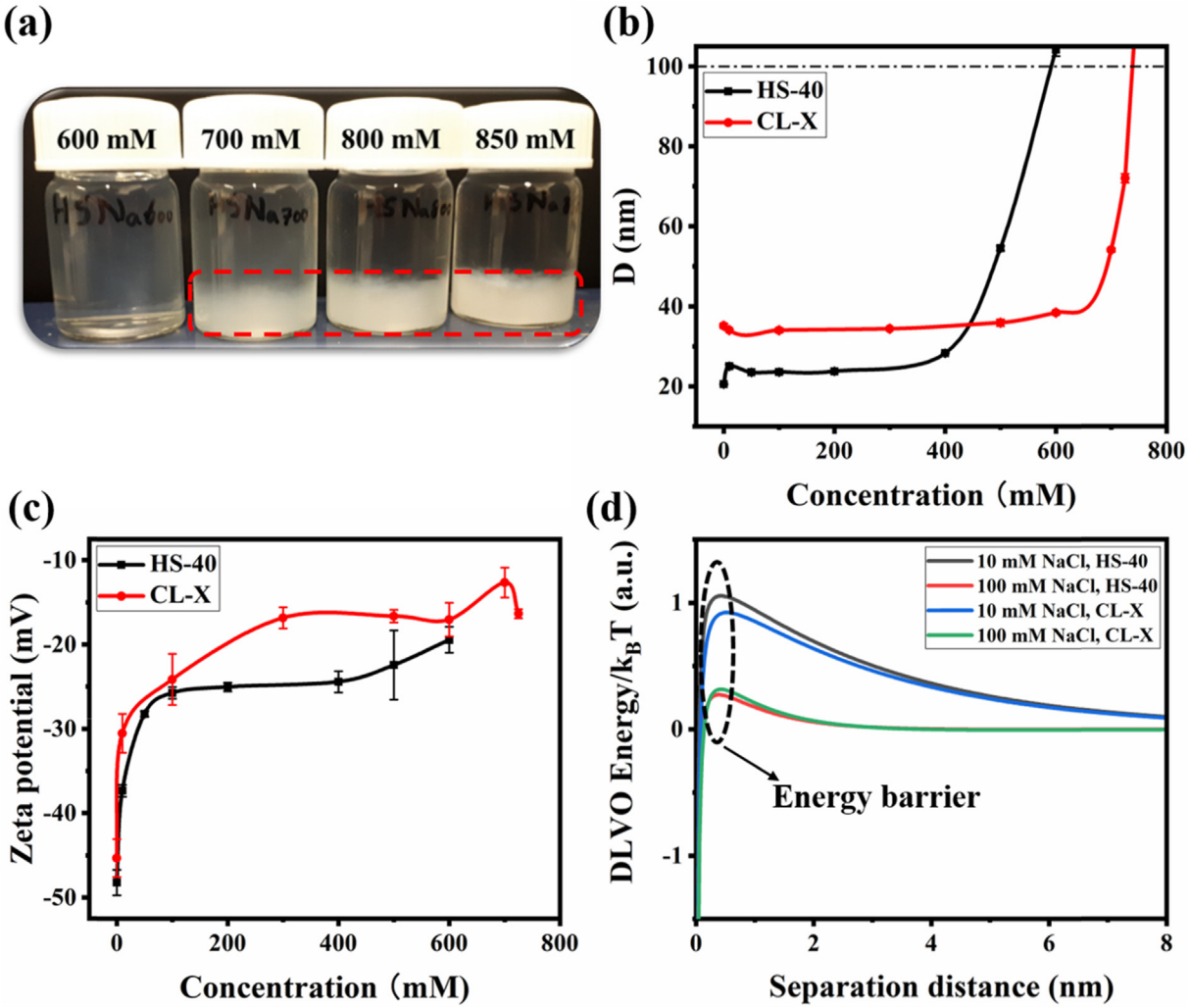

Fig. 2. (a) The visual status of HS-40 silica nanoparticles in various concentrations of NaCl solutions after 48 h, and the red dash line indicates the formation of HS-40 precipitations. (b) DLS analysis of size and (c) LDE zeta potential of HS-40 and CL-X silica nanoparticles dispersed in the aqueous solution with varying NaCl concentrations, at pH 9.5. (d) DLVO energy calculation for silica nanoparticles interactions as function of separation distance in the presence of different concentrations of NaCl. The black dash circle indicates peaks of energy barriers, which silica nanoparticles need to overcome before aggregation. (For interpretation of the references to colour in this figure legend, the reader is referred to the web version of this article.)

Table 1
The critical aggregation concentrations (in mM) of HS-40 and CL-X silica nanoparticles at pH 9.5.

	NaCl	$CaCl_2$	$MgCl_2$
HS-40	500–600	2.5–3.0	1.5–2.0
CL-X	750–800	2.0–2.5	1.25–1.5

interaction likely played a dominant role in this comparison. As NaCl concentration was increased from 10 to 100 mM, the Debye length was correspondingly decreased from 3.04 to 0.96 nm. The decreased Debye length implicated the less EDL thickness and more Na^+ could cover around SNP surfaces. A much less zeta potential confirmed this speculation. From 10 to 100 mM NaCl, the zeta potential of HS-40 and CL-X decreased from −37 to −26 mV and −31 to −24 mV, respectively. Moreover, at 10 mM NaCl, the repulsive energy barrier was obviously higher for HS-40 than CL-X, which was consistent with a smaller particle size for HS-40. Even the size of CL-X was larger than HS-40 in 100 mM NaCl, their zeta potentials were almost the same in the range of errors. Based on the DLVO calculations, the EDL interaction contributed more to the energy barriers in 100 mM NaCl.

3.2.2. Reversibility

It is also interesting to know whether the SNP aggregation process is reversible or not. Two situations were chosen. One was that the SNP had intense aggregation with the formation of precipitations. The other was to choose the light SNP aggregation with particle size smaller than 100 nm. As expected, HS-40 was highly unstable in the 1000 mM NaCl solution, as can be seen by the clear precipitations in Fig. S1. The 1000 mM NaCl solution was later diluted 10 times into a pair of 100 mM NaCl solutions as described in Section 2.4. There were some visible precipitations for both sonicated and non-sonicated 100 mM NaCl with HS-40. This suggests that the sonication was unsuccessful in reversing the salt-induced aggregation. The HS-40 from the 1000 mM NaCl solution was still severely aggregated after dilution and the increased EDL repulsive force was not enough to overcome the tightly binding among SNPs.

A similar experiment was performed on the 500 mM NaCl solution containing HS-40. After 10 times dilution into 50 mM NaCl solutions, all these solutions were visually stable. Their size distribution was measured, with a mean diameter of 69.4 ± 1 nm for 500 mM NaCl, and 35.8 ± 0.8 nm and 36.6 ± 0.6 nm for the sonicated and non-sonicated 50 mM NaCl solutions, respectively. These values were higher than the values obtained in the previous section of HS-40 in the presence of 500 and 50 mM NaCl with the size of 54.5 ± 0.6 and 23.6 ± 0.2 (Fig. 2b), respectively. The size difference between HS-40 in 500 mM NaCl solutions can be attributed to the different waiting times (48 and 72 h). HS-40 was likely still aggregating after 48 h, showing a larger mean diameter (about 15 nm more) in 72 h. Moreover, a smaller HS-40 size was exhibited in 50 mM NaCl from diluting 500 mM NaCl solution, indicating the light aggregation process was reversed. A slight difference in HS-40 size was found with and without sonication. However, their sizes were about 13 nm larger than the previous value of 23.6 ± 0.2 in 50 mM NaCl. From these comparisons, a general conclusion can be drawn that the light aggregation of HS-40 in 500 mM NaCl is partially reversible, while the serious aggregation is irreversible in 1000 mM NaCl.

3.2.3. $CaCl_2$ and $MgCl_2$ solutions

We now come to the point of the effect of divalent cations on the aggregation behaviour of SNPs. Fig. 3a and b show the size and zeta potential of SNPs in the solutions containing different $CaCl_2$ concentrations. The size of both SNPs had slight changes between 0 and 1 mM, followed by a rapid increase with increasing $CaCl_2$ concentrations. At the same concentration of $CaCl_2$, the size of CL-X was always larger than HS-40. This can be due to the larger particle size of CL-X to bind more divalent cations, resulting in less repulsive force among SNPs. The CAC for HS-40 and CL-X in the presence of $CaCl_2$ is 2.5–3.0 and 2.0–2.5 mM, respectively. It can be seen from the zeta potential curves that the tendency change of HS-40 and CL-X in $CaCl_2$ was quite similar to the curves in NaCl (Fig. 2c). Above 0.5 mM $CaCl_2$, the zeta potential was in the order of −20 mV. In Fig. 3c, the size change in $MgCl_2$ resembled in $CaCl_2$ of Fig. 3a, as well as its zeta potential curves (Fig. S2) to the Fig. 3b. The CAC values for $MgCl_2$ were found to be in the ranges of 1.5–2.0 mM for HS-40, and 1.25–1.5 mM for CL-X. In comparison with obtained CACs (Table 1), the aggregate size of SNPs was much more sensitive to the presence of $MgCl_2$ than $CaCl_2$.

The difference of CAC in $MgCl_2$ and $CaCl_2$ was further examined by the DLVO theory. Fig. 3d presented the normalized interaction energy between two identical SNPs as a function of the separation distance in the presence of 0.5 mM $MgCl_2$ and $CaCl_2$. The Debye length in this case was 7.9 nm. The DLVO energy curves were relatively flat compared to in NaCl (Fig. 2d), indicating small energy barriers for SNPs. It can be seen that the energy barrier was the smallest for HS-40 in $CaCl_2$ and the largest HS-40 in $MgCl_2$. However, these calculations failed to explain the observed CAC order of SNPs in different divalent cation solutions, indicating that the interaction among SNPs was a more complex process rather than only a simple EDL suppression process. Additionally, the CACs for both $MgCl_2$ and $CaCl_2$ were much lower than the CAC of NaCl. Mg^{2+} and Ca^{2+} are divalent cations, and are therefore capable of cation bridging. This can be the main reason for this lower CACs and also explains the difference between the two divalent salts, as Mg^{2+} has a smaller ionic radius than Ca^{2+}, but equal charge. Cation bridging is stronger for smaller ions with higher charge; thus, the reaction strength of Mg^{2+} is stronger than Ca^{2+} [58,59]. Therefore, a lower CAC was obtained in $MgCl_2$. From the view of the hydration force, smaller cations can more easily penetrate into the bound water layer of the SNPs, leading to less repulsive force compared to larger ions that resided outside the hydration layer [51,60]. Our observations on the stability of SNP dispersions were consistent with this theory. Mg^{2+} being the smaller cation with higher affinity to water-induced the smaller repulsive force and exhibited the less CAC compared to Ca^{2+}.

3.3. Effect of anionic AAS surfactant

To examine the effect of a commonly used AAS anionic surfactant on the stability of SNPs, the aggregation behaviour of SNPs was investigated in various salt solutions at room temperature, and at pH = 9.5. Fig. 4a and b show how 0.15 wt% AAS affected the size and zeta potential of CL-X in NaCl. Below 500 mM NaCl, the size curves of CL-X were nearly overlapped in the absence and presence of AAS. However, CL-X exhibited less tolerance to the high concentration of NaCl, with a smaller CAC between 500 and 550 mM NaCl in 0.15 wt% AAS. Yet despite this, the zeta potential was higher than without AAS. It is expected that a stronger repulsive interaction resulted in a larger CAC for CL-X with AAS. However, the contrary was found and a possible explanation of this discrepancy may be found in the behaviour of the AAS in aqueous environments. The used concentration of AAS lies very well above its critical micelle concentration [61], and therefore the AAS would be mainly present in the form of negatively charged micelles. These micelles were expected to behave similarly to the CL-X, with also a negative charge on its surface. These micelles could then form their own EDL, contributing to the measured zeta potential. The addition of AAS did not influence the DLS measurements. The estimated size of AAS micelle was around 6 nm (twice the molecular length) and such AAS size peak was not observed in any of the samples. Additionally, the presence of the charged AAS created a negative background potential, meaning that electrostatic repulsion between the CL-X and AAS would push SNPs together, which acted as an additional force promoting collisions and aggregation, especially in higher NaCl concentrations. This was the likely reason why we found smaller CAC with AAS.

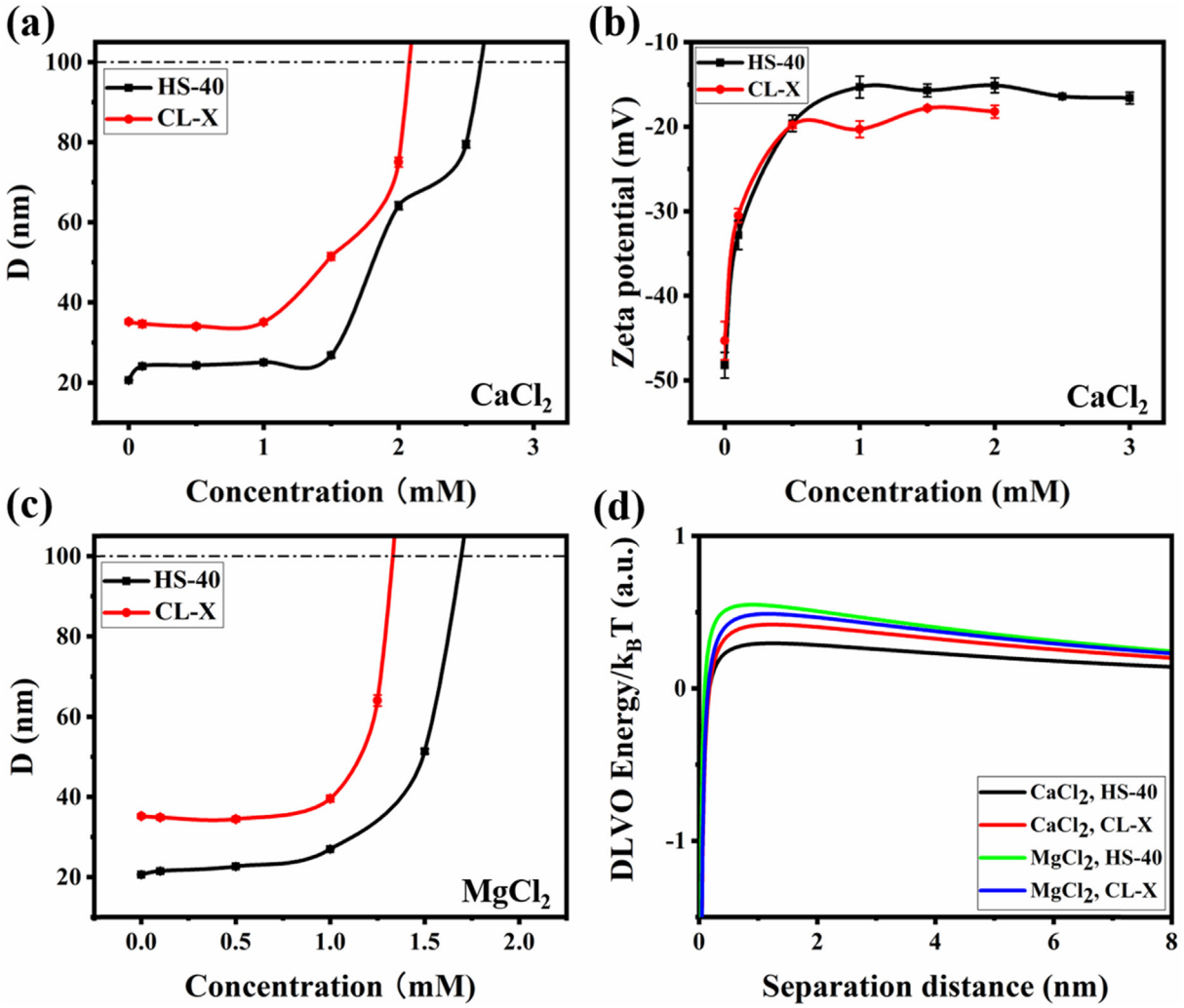

Fig. 3. (a) DLS analysis of size and (b) LDE zeta potential of HS-40 and CL-X silica nanoparticles dispersed in varying $CaCl_2$ concentrations, at pH 9.5. (c) DLS analysis of HS-40 and CL-X size in varying $MgCl_2$ concentrations. (d) DLVO energy calculation for silica nanoparticles in the presence of 0.5 mM $CaCl_2$ and $MgCl_2$.

Next we come to the presence of divalent cations in Fig. 4b and c. It can be seen that the AAS had only a slight effect on the size of CL-X in $CaCl_2$ solution and almost no effect in $MgCl_2$ solution. The CAC of CL-X was 1.5–2.0 mM of $CaCl_2$ in 0.15 wt% AAS, which was a bit smaller than 2.0–2.5 mM of $CaCl_2$ in the absence of AAS. The size curve in $CaCl_2$ diverged at concentrations higher than 1.5 mM and an AAS solution containing 2.0 mM $CaCl_2$ was visually unstable. Their zeta potentials were similar to the potentials observed in NaCl, noticeably a bit more negative (Fig. S3). Initially, it was expected that the divalent cations would bridge the AAS molecules to CL-X, thereby introducing steric stabilization. But if this were indeed the case, this would have come paired with a decrease in size for the CL-X, which was not observed. From this it can be concluded that the AAS was not grafted onto the CL-X surface. Overall, the presence of AAS surfactant had a slightly negative effect on the stability of the SNP solutions.

3.4. Effect of PA polyanion

3.4.1. Salt solutions

In this section, we investigated the effect of the polyanion PA on the stability of HS-40, at room temperature and pH 9.5. Similar to AAS in NaCl, PA has a negligible effect on the size of HS-40. Therefore, more attention was put on the effect of PA in $CaCl_2$ and $MgCl_2$ solutions. Fig. 5 shows the effect of varying concentrations of PA on the size of HS-40 in the presence of $CaCl_2$. It was found that the change of HS-40 size at various PA concentrations followed a similar tendency as in the absence of PA. The size of HS-40 started nearly constant until a certain $CaCl_2$ concentration, with a rapid increase as the particles started obviously aggregating. With the increase of PA concentration, the CAC for HS-40 correspondingly increased. At 100 ppm PA, the CAC was 15–17 mM $CaCl_2$, which was 5 times more than its value in the absence of PA. Indeed, PA greatly stabilized the HS-40. Likely, the PA was grafted onto the HS-40 surface that was different from AAS. This grafting also explained the zeta potential differences between the PA concentrations in Fig. 5b, as the grafting of PA molecules introduced more anionic groups. The observed increase in stability probably originated from the increased hydration force caused by the PA's negative charge. A similar PA effect on the size of HS-40 in $MgCl_2$ solutions was found in Fig. 5c. The obtained results of CACs in $MgCl_2$ were also found to be smaller in $CaCl_2$, which can be found in Table 2.

With these results, it has not only been shown that PA improves the HS-40 stability, it also opens the possibility of PA actively being used as a stabilizing agent. If this were to be done, it needs to be considered that PA stabilizes only in the presence of divalent cations, as without their cation bridging, the negatively charged PA would not be grafted onto the negatively charged SNPs. This means that PA is only usable in solutions with significant concentrations of divalent cations, or that divalent cations need to be introduced alongside the PA, preferably before exposure to monovalent cations, as to limit the amount of competition. It should be kept in mind that this grafting of PA is kind of a surface

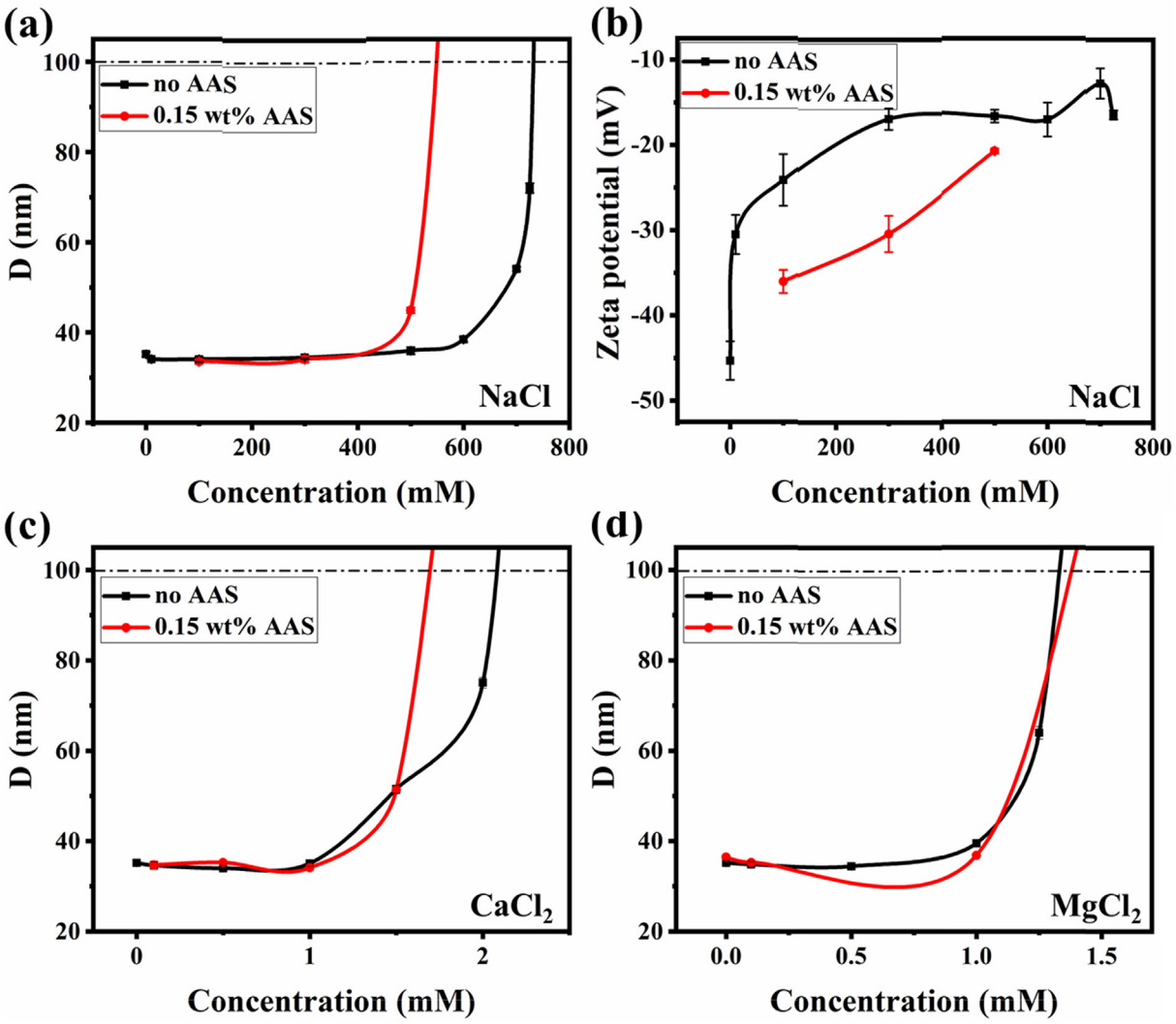

Fig. 4. (a) DLS analysis of size and (b) LDE zeta potential of CL-X silica nanoparticles dispersed in the absence of AAS and in the presence of 0.15 wt% AAS in varying NaCl concentrations, at pH 9.5. DLS analysis of CL-X in varying (c) $CaCl_2$ and (d) $MgCl_2$ concentrations.

modification, as shown in Fig. 5d, thereby introducing steric stabilization. In cEOR applications, no special surface modification needs to be done if the added surfactants or polymer could be grafted to SNPs surfaces.

3.4.2. pH effect

In order to investigate how far the stabilization of HS-40 could go, 50 mM $MgCl_2$ solutions were chosen, as this was close to $MgCl_2$ concentration in seawater [58]. All of the prepared solutions with PA (250–1000 ppm, as described in Section 2.5) were initially stable, and it became unstable as solution pH was increased, during which the solutions rapidly and visually aggregated, and shifted from a clear state to be cloudy. The pH values at which this occurred were around pH 8.9, 9.4, 9.5, and 9.5 for 250, 500, 750, and 1000 ppm PA, respectively. It is assumed that the pH at which the solutions become unstable can be used as a rough indication of stability, it showed that 500 ppm PA nearly stabilized HS-40 in the 50 mM $MgCl_2$ solution, which was enough to prevent aggregation at pH 9.5. It also showed that the addition of more PA above this concentration did not improve the cloudy pH in 50 mM $MgCl_2$, making it unlikely, or unfeasible, for PA alone to act as a stabilizing agent in these conditions. Alternatively, the stabilization might be further enhanced by using polymers with a larger molecular weight, as this would increase the steric stabilization it provides.

We also performed experiments on a solution containing 0.3 wt% HS-40, 300 ppm PA, and 50 mM $CaCl_2$. In Fig. 6, there was no significant effect on the size below pH 8.5. However, the solution was visually unstable at pH 9. This means that at a pH above 8.5, the particles rapidly aggregated. The pH was indeed a factor determining the stability of the nanoparticles, and that a lower pH was more favourable. Lowering the pH of the solution from 9.5 to 8.5 can stabilize the HS-40 solution at higher salinity. This was consistent with the proposed proton protection in Section 2.6. In Fig. 6b, the zeta potential of HS-40 increased with increasing pH. The lower potential did not mean the instability of HS-40. PA was prone easily to cover the surface of HS-40 at low pH, thus the repulsive hydration force and steric interactions were more important to inhibit the aggregation. Moreover, we investigated the stability of HS-40 in mixed high salinity solutions containing both 50 mM $CaCl_2$ and 500 mM NaCl. Two solutions contained 300 ppm PA at pH 8.5 and 9, while the other two contained 350 ppm PA also at pH 8.5 and 9. Of the four solutions, 350 ppm PA at pH 8.5 was the only stable solution without precipitations. This simple inspection also confirmed PA effect and proton protection in low pH for the stability of SNPs.

4. Conclusions

The use of SNPs in EOR is currently an active area of investigation. The key to the successful SNP application depends on its stability in

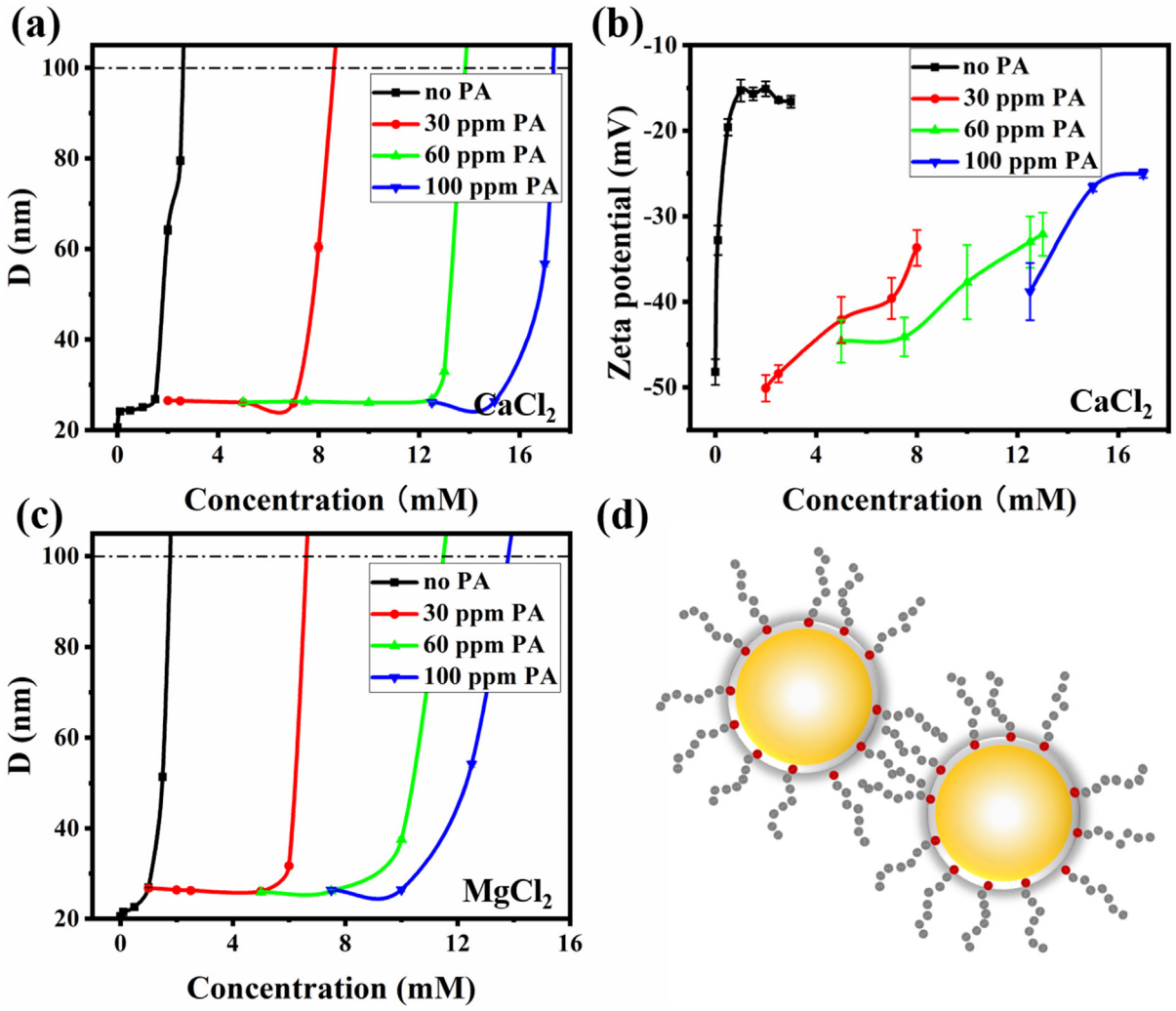

Fig. 5. (a) DLS analysis of size and (b) LDE zeta potential of HS-40 silica nanoparticles dispersed in various PA concentrations as a function of $CaCl_2$ concentrations, at pH 9.5. (c) DLS analysis of size of HS-40 silica nanoparticles dispersed in $MgCl_2$. (d) Schematic illustration of the adsorbed PA polyelectrolytes on nanoparticle surfaces.

Table 2
The critical aggregation concentrations (in mM) of HS-40 silica nanoparticles in varying PA concentrations, at pH 9.5.

PA	0 ppm	30 ppm	60 ppm	100 ppm
NaCl	500–600	500–600	–	–
$MgCl_2$	1.5–2.0	6–7	10–12.5	12.5–15
$CaCl_2$	2.5–3.0	8–9	13–15	17–18

various EOR environments. In this study, the stability of SNPs was examined in aqueous solutions under changing pH, salt concentrations, anionic AAS surfactants and PA polyelectrolytes. Increasing solution pH, the zeta potential of SNPs increased, but no accompanying change in size was observed at any of the investigated pH values. It was found that the CAC for NaCl was above 500 mM and DLVO well explained the size change of SNPs in different NaCl concentrations. The reversibility of SNP aggregation process was evaluated in 500 and 1000 mM NaCl. The light aggregation in 500 mM NaCl was partially reversible, while the intense aggregation was irreversible in 1000 mM NaCl. In divalent cation solutions, the CAC (about 2 mM) for $CaCl_2$ was greater than $MgCl_2$. DLVO calculations failed to explain the observed CAC order and the non-DLVO interactions such as cation bridging, steric effect, and hydration force should be considered. Moreover, the presence of AAS surfactant slightly destabilized the SNP solutions and this was regarded as caused by the anionic compounds creating a negative background potential, which promoted collisions and aggregation among SNPs. Additionally, PA greatly stabilized SNPs and the CAC for $CaCl_2$ and $MgCl_2$ increased with increasing PA. Upon addition of 100 ppm PA, CAC improved 5 times with divalent cations (17–18 mM for $CaCl_2$ and 12.5–15 mM for $MgCl_2$) compared to the absence of PA. This was because of the PA polyanionic properties increasing the hydration force of SNPs and steric stabilization. However, PA was only grafted onto the SNP surface in the presence of divalent cations, as it relied on cation bridging. By reducing solution pH, SNP can be stabilized in higher salinity with the addition of a tiny amount of PA. The results of this study provided a basic understanding of SNP stability and contributed to a more efficient use of SNP in EOR.

Authors' contributions

Z.L. and E.J.R.S. supervised the whole work and were involved in funding acquisition and project administration. Z.L., V.B., and P.H. conceptualized the study and devised the stability of silica nanoparticles experiments. With the help of Z.L. P.H. and H.O., V.B. conducted visual inspections, size measurements, and zeta potential measurements. Z.L., P.H., and H.O. did theoretical calculaitons with DLVO modelling. Z.L., V.B., and E.J.R.S. analyzed the data and wrote the paper with input from all authors. All authors contributed to scientific

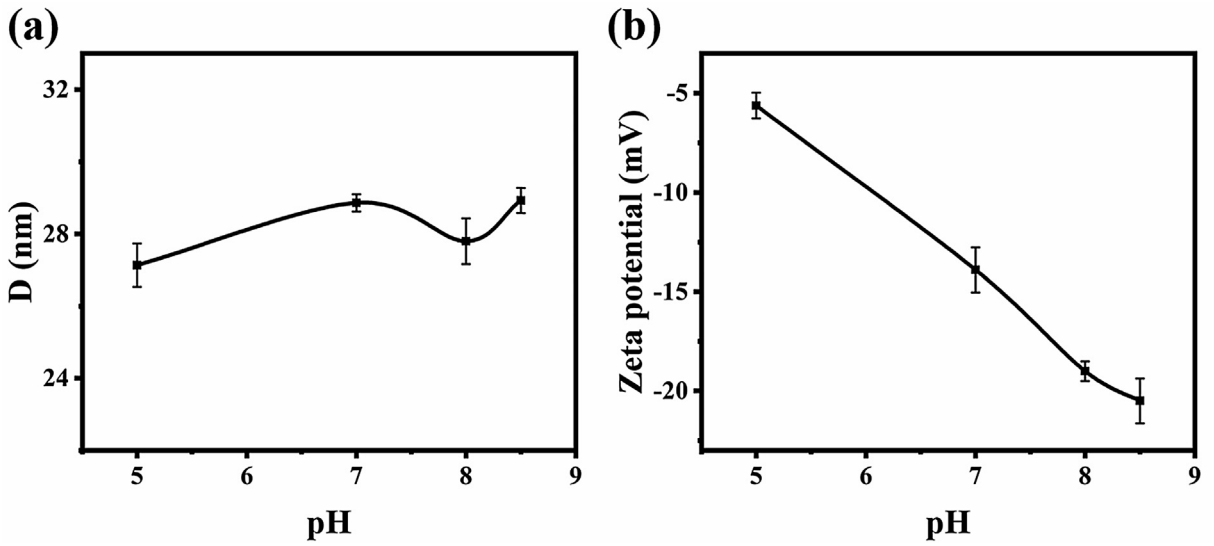

Fig. 6. (a) DLS analysis of size and (b) LDE zeta potential of HS-40 silica nanoparticles dispersed in 300 ppm PA, 50 mM $CaCl_2$ solutions with as a function of solution pH.

discussions and analysis, and have approved the final version of the manuscript.

Declaration of Competing Interest

The authors declare that they have no known competing financial interests or personal relationships that could have appeared to influence the work reported in this paper.

Acknowledgments

The authors thank Dr. M. Brewer, Dr. Dirk Groenendijk, and Dr. J. van Wunnik (Shell Global Solutions) for providing surfactant samples and for their active discussions. Technical assistance from Mr. Duco Bosma and Mr. Marcel Bus of TU Delft is highly appreciated. Financial support was provided by Shell Global Solutions.

Appendix A. Supplementary data

Supplementary data to this article can be found online at https://doi.org/10.1016/j.fuel.2020.118650.

References

[1] Rezk MY, Allam NK. Impact of nanotechnology on enhanced oil recovery: a mini-review. Ind. Eng. Chem. Res. 2019;58(36):16287–95.
[2] Kamal MS, Adewunmi AA, Sultan AS, Al-Hamad MF, Mehmood U. Recent advances in nanoparticles enhanced oil recovery: rheology, interfacial tension, oil recovery, and wettability alteration. J. Nanomater. 2017;2017.
[3] Gbadamosi AO, Junin R, Manan MA, Yekeen N, Agi A, Oseh JO. Recent advances and prospects in polymeric nanofluids application for enhanced oil recovery. J. Ind. Eng. Chem. 2018;66:1–19.
[4] Agi A, Junin R, Gbadamosi A. Mechanism governing nanoparticle flow behaviour in porous media: insight for enhanced oil recovery applications. Int. Nano Lett. 2018;8(2):49–77.
[5] Hirasaki G, Miller CA, Puerto M. Recent Advances in Surfactant EOR. SPE J. 2011;16(04):889–907.
[6] Lake LW., Johns RT, Rossen WR, Pope GA. Fundamentals of enhanced oil recovery, 2014.
[7] Tagavifar M, Jang SH, Sharma H, Wang D, Chang LY, Mohanty K, et al. Effect of PH on adsorption of anionic surfactants on limestone: experimental study and surface complexation modeling. Colloids Surf. Physicochem. Eng. Asp. 2018;538:549–58.
[8] Elias SD, Rabiu AM, Oluwaseun O, Seima B. Adsorption characteristics of surfactants on different petroleum. Online J Sci Technol 2016;6(4):6–16.
[9] Ahmadi MA, Shadizadeh SR. Experimental investigation of a natural surfactant adsorption on shale-sandstone reservoir rocks: static and dynamic conditions. Fuel 2015;159:15–26.
[10] Almahfood M, Bai B. The synergistic effects of nanoparticle-surfactant nanofluids in EOR Applications. J. Pet. Sci. Eng. 2018;171:196–210.
[11] Wang Z, Yu T, Lin X, Wang X, Su L. Chemicals loss and the effect on formation damage in reservoirs with ASP flooding enhanced oil recovery. J. Nat. Gas Sci. Eng. 2016;33:1381–9.
[12] Negin C, Ali S, Xie Q. Most common surfactants employed in chemical enhanced oil recovery. Petroleum 2017;3(2):197–211.
[13] Yekeen N, Manan MA, Idris AK, Samin AM, Risal AR. Experimental investigation of minimization in surfactant adsorption and improvement in surfactant-foam stability in presence of silicon dioxide and aluminum oxide nanoparticles. J. Pet. Sci. Eng. 2017;159:115–34.
[14] Zargartalebi M, Kharrat R, Barati N. Enhancement of surfactant flooding performance by the use of silica nanoparticles. Fuel 2015;143:21–7.
[15] Abhishek R, Hamouda AA, Murzin I. Adsorption of silica nanoparticles and its synergistic effect on fluid/rock interactions during low salinity flooding in sandstones. Colloids Surf. Physicochem. Eng. Asp. 2018;555:397–406.
[16] Jha NK, Iglauer S, Barifcani A, Sarmadivaleh M, Sangwai JS. Low-salinity surfactant nanofluid formulations for wettability alteration of sandstone: role of the SiO2 nanoparticle concentration and divalent cation/SO42–ratio. Energy Fuels 2019;33(2):739–46.
[17] Gbadamosi AO, Junin R, Abdalla Y, Agi A, Oseh JO. Experimental investigation of the effects of silica nanoparticle on hole cleaning efficiency of water-based drilling mud. J. Pet. Sci. Eng. 2019;172:1226–34.
[18] Wu Y, Chen W, Dai C, Huang Y, Li H, Zhao M, et al. Reducing surfactant adsorption on rock by silica nanoparticles for enhanced oil recovery. J. Pet. Sci. Eng. 2017;153:283–7.
[19] Hashemi R, Nassar NN, Almao PP. Nanoparticle technology for heavy oil in-situ upgrading and recovery enhancement: opportunities and challenges. Appl. Energy 2014;133:374–87.
[20] Sun X, Zhang Y, Chen G, Liu T, Ren D, Ma J, et al. Wettability of hybrid nanofluid-treated sandstone/heavy oil/brine systems: implications for enhanced heavy oil recovery potential. Energy Fuels 2018;32(11):11118–35.
[21] Al-Anssari S, Wang S, Barifcani A, Lebedev M, Iglauer S. Effect of temperature and SiO2 nanoparticle size on wettability alteration of oil-wet calcite. Fuel 2017;206:34–42.
[22] Mandal A, Bera A, Ojha K, Kumar T. Characterization of Surfactant Stabilized Nanoemulsion and Its Use in Enhanced Oil Recovery. Society of Petroleum Engineers; 2012.
[23] Arab D, Pourafshary P. Nanoparticles-assisted surface charge modification of the porous medium to treat colloidal particles migration induced by low salinity water flooding. Colloids Surf. Physicochem. Eng. Asp. 2013;436:803–14.
[24] Zhang H, Nikolov A, Wasan D. Enhanced oil recovery (EOR) using nanoparticle dispersions: underlying mechanism and imbibition experiments. Energy Fuels 2014;28(5):3002–9.
[25] Zhang T, Roberts M, Bryant SL, Huh C. Foams and emulsions stabilized with nanoparticles for potential conformance control applications. SPE international symposium on oilfield chemistry. Society of Petroleum Engineers; 2009.
[26] Singh SK, Ahmed RM, Growcock F. Vital role of nanopolymers in drilling and stimulations fluid applications. SPE annual technical conference and exhibition. Society of Petroleum Engineers; 2010.
[27] Li S, Torsaeter O. The Impact of Nanoparticles Adsorption and Transport on Wettability Alteration of Intermediate Wet Berea Sandstone. Society of Petroleum Engineers; 2015.
[28] Miranda CR, Lara LS, de Tonetto BC. Stability and mobility of functionalized silica nanoparticles for enhanced oil recovery applications. SPE international oilfield nanotechnology conference and exhibition. Society of Petroleum Engineers; 2012.
[29] Yu W, Wang T, Park A-HA, Fang M. Review of liquid nano-absorbents for enhanced

CO 2 Capture. Nanoscale 2019;11(37):17137–56.
[30] Nguyen P, Fadaei H, Sinton D. Pore-scale assessment of nanoparticle-stabilized CO2 foam for enhanced oil recovery. Energy Fuels 2014;28(10):6221–7.
[31] Clark JA, Santiso EE. Carbon sequestration through CO2 foam-enhanced oil recovery: a green chemistry perspective. Engineering 2018;4(3):336–42.
[32] Adil M, Zaid HM, Chuan LK, Latiff NRA. Effect of dispersion stability on electrorheology of water-based ZnO nanofluids. Energy Fuels 2016;30(7):6169–77.
[33] Maghzi A, Kharrat R, Mohebbi A, Ghazanfari MH. The impact of silica nanoparticles on the performance of polymer solution in presence of salts in polymer flooding for heavy oil recovery. Fuel 2014;123:123–32.
[34] Lv Q, Zhou T, Zhang X, Zuo B, Dong Z, Zhang J. Enhanced oil recovery using aqueous CO2 foam stabilized by particulate matter from coal combustion. Energy Fuels 2020;34(3):2880–92.
[35] Mohajeri M, Hemmati M, Shekarabi AS. An experimental study on using a nano-surfactant in an EOR process of heavy oil in a fractured micromodel. J. Pet. Sci. Eng. 2015;126:162–73.
[36] Al-Anssari S, Arif M, Wang S, Barifcani A, Iglauer S. Stabilising nanofluids in saline environments. J. Colloid Interface Sci. 2017;508:222–9.
[37] Esfandyari Bayat A, Junin R, Samsuri A, Piroozian A, Hokmabadi M. Impact of metal oxide nanoparticles on enhanced oil recovery from limestone media at several temperatures. Energy Fuels 2014;28(10):6255–66.
[38] Olayiwola SO, Dejam M. A comprehensive review on interaction of nanoparticles with low salinity water and surfactant for enhanced oil recovery in sandstone and carbonate reservoirs. Fuel 2019;241:1045–57.
[39] El-sayed GM, Kamel MM, Morsy NS, Taher FA. Encapsulation of nano disperse red 60 via modified miniemulsion polymerization. I. Preparation and characterization. J. Appl. Polym. Sci. 2012;125(2):1318–29.
[40] ShamsiJazeyi, H.; Miller, C. A.; Wong, M. S.; Tour, J. M.; Verduzco, R. Polymer-coated nanoparticles for enhanced oil recovery. J. Appl. Polym. Sci. 2014, 131 (15).
[41] Al-Anssari S, Wang S, Barifcani A, Iglauer S. Oil-water interfacial tensions of silica nanoparticle-surfactant formulations. Tenside Surfactants Deterg. 2017;54(4):334–41.
[42] Sharma T, Kumar GS, Sangwai JS. Comparative effectiveness of production performance of pickering emulsion stabilized by nanoparticle–surfactant–polymerover surfactant-polymer (SP) flooding for enhanced oil recoveryfor brownfield reservoir. J. Pet. Sci. Eng. 2015;129:221–32.
[43] Somasundaran P, Mehta SC, Yu X, Krishnakumar S. Colloid systems and interfaces stability of dispersions through polymer and surfactant adsorption. Handbook of Surface and Colloid Chemistry. CRC Press; 2008. p. 162–203.
[44] Kazemzadeh Y, Shojaei S, Riazi M, Sharifi M. Review on application of nanoparticles for EOR purposes: a critical review of the opportunities and challenges. Chin. J. Chem. Eng. 2019;27(2):237–46.
[45] Nelson PH. Pore-throat sizes in sandstones, tight sandstones, and shales. AAPG Bull. 2009;93(3):329–40.
[46] Horikoshi S, Serpone N. Microwaves in Nanoparticle Synthesis: Fundamentals and Applications. John Wiley & Sons; 2013.
[47] Adkins S, Liyanage PJ, Arachchilage P, Gayani WP, Mudiyanselage T, Weerasooriya U, et al. A new process for manufacturing and stabilizing high-performance eor surfactants at low cost for high-temperature, High-Salinity Oil Reservoirs. SPE Improved Oil Recovery Symposium. Society of Petroleum Engineers; 2010.
[48] Israelachvili JN. Intermolecular and Surface Forces. Academic press; 2011.
[49] Ueno K, Inaba A, Kondoh M, Watanabe M. Colloidal stability of bare and polymer-grafted silica nanoparticles in ionic liquids. Langmuir 2008;24(10):5253–9.
[50] Clogston JD, Patri AK. Zeta potential measurement. Characterization of Nanoparticles Intended for Drug Delivery. Springer; 2011. p. 63–70.
[51] Metin CO, Lake LW, Miranda CR, Nguyen QP. Stability of aqueous silica nanoparticle dispersions. J. Nanoparticle Res. 2011;13(2):839–50.
[52] Jenkins S, Kirk SR, Persson M, Carlen J, Abbas Z. Molecular dynamics simulation of nanocolloidal amorphous silica particles: Part II. J. Chem. Phys. 2008;128(16):164711.
[53] Liu Z, Rios-Carvajal T, Andersson MP, Stipp S, Hassenkam T. Ion effects on molecular interaction between graphene oxide and organic molecules. Environ. Sci. Nano 2019;6(7):2281–91.
[54] Higgins MJ, Novak JT. The effect of cations on the settling and dewatering of activated sludges: laboratory results. Water Environ. Res. 1997;69(2):215–24.
[55] Elimelech M, Gregory J, Jia X. Particle Deposition and Aggregation: Measurement, Modelling and Simulation. Butterworth-Heinemann; 2013.
[56] Sofla SJD, James LA, Zhang Y. Insight into the stability of hydrophilic silica nanoparticles in seawater for enhanced oil recovery implications. Fuel 2018;216:559–71.
[57] Sögaard C, Funehag J, Abbas Z. Silica sol as grouting material: a physio-chemical analysis. Nano Converg. 2018;5(1):6.
[58] Liu ZL, Rios-Carvajal T, Andersson MP, Ceccato M, Stipp SLS, Hassenkam T. Insights into the pore-scale mechanism for the low-salinity effect: implications for enhanced oil recovery. Energy Fuels 2018;32(12):12081–90.
[59] Arnarson TS, Keil RG. Mechanisms of pore water organic matter adsorption to montmorillonite. Mar. Chem. 2000;71(3–4):309–20.
[60] Torrie GM, Kusalik PG, Patey GN. Theory of the electrical double layer: ion size effects in a molecular solvent. J. Chem. Phys. 1989;91(10):6367–75.
[61] Liu Z, Ghatkesar MK, Sudholter EJ, Singh B, Kumar N. Understanding the cation dependent surfactant adsorption on clay minerals in oil recovery. Energy Fuels 2019;33(12):12319–29.